Acoustic Field-assisted Particle Patterning for Smart Polymer Composite Fabrication in Stereolithography

Lu Lu[a], Xiaohui Tang[b], Shan Hu[b] and Yayue Pan[a]*

[a] Department of Mechanical and Industrial Engineering, The University of Illinois at Chicago, Chicago, IL, 60607, United States

[b] Department of Mechanical Engineering, Iowa State University, Ames, IA, 50011, United States

* Corresponding Author: yayuepan@uic.edu

Abstract

By combining various materials that serve mechanical, electrical, chemical, and thermal functions with controlled local distributions, smart devices and machines with multiple functionalities can be fabricated. This paper reports a new particle patterning approach during additive manufacturing to fabricate multi-functional smart composite objects. An acoustic field is integrated into the projection based stereolithography system to pattern different micro-particles into dense parallel curves or networks in the liquid resin. Effects of acoustic field settings and manufacturing process parameters on patterning are modeled and experimentally characterized. Various particle patterning results are presented. An acoustic field assisted projection stereolithography testbed has been developed. The feasibility of the proposed approach for multi-functional particle-polymer composite fabrication has been verified.

Keywords: Mask image projection stereolithography, Particle-polymer composite, Acoustic field, Particle patterning

1. Introduction

Multi-material functional particle-polymer composites can be obtained by combining functional particles with polymer. The resulting component is characterized by enhanced mechanical properties and a higher degree of functionality. Based on different material characters, it can be categorized into two types. The first type is homogeneous with uniform distribution of particles, such as reinforced polymer [1]. Heterogeneous with anisotropy is the second type. The anisotropic property is usually determined by orientations/alignments of the particles as demonstrated in biomimetic materials [2]. Functionally graded material with anisotropic property proves that anisotropy also depends on local composition [3, 4].

Compared to traditional manufacturing processes such as machining and molding, Multi-material Additive Manufacturing technology can enable the full functionality of heterogeneous particle-polymer composites and allow a higher degree of design, by controlling orientations/alignments and local compositions of particles in the polymer matrix. According to particle manipulation method, multi-material additive manufacturing processes for fabrication of heterogeneous particle-polymer composites can be classified into two groups: shear-flow induced process, and external field induced process, such as electrical field and magnetic field. Compton et al. [5] demonstrated that fillers could be oriented along the printing direction by the shear flow and a lightweight cellular composite was obtained by direct writing technique. However, such shear induced process limits material selection to fibers. Furthermore, due to nozzle clogging issues, only composites with a very limited loading fraction of fibers can be fabricated. Yang et al. [2] integrated a rotating electrical field with projection based stereolithography (SL) to fabricate bio-inspired composites. This process allows a wider choice of materials and works for not only fibers, but also spherical and non-spherical particles. Yet the condition is that particle has to be charged in advance. Additionally,

the particle distribution cannot be controlled locally, since the entire printing area was covered by a uniform electrical field. Magnetic field induced processes utilize the magnetic field to control the particle orientation in fabrication of magnetic-field-responsive composites [6] and bioinspired composites [7]. Local particle composition control by using a moving magnetic field was also demonstrated [8-9]. A major limitation of these external field-assisted process is that the particles have to be naturally responsive to the applied external field. Otherwise, the particles have to be surface coated with magnetic responsive nanoparticles and maybe still cannot be processed by the manufacturing technique. Pan *et al.* proposed a method of integrating electrostatic deposition with stereolithography to fabricate particle-polymer composites with locally controlled particle composition [10]. In those work, most methods can either only align or orient particles in the polymer matrix, or only control the local composition. Very few of them are able to simultaneously control the orientation and local composition of particles, thus significantly limiting the domain of the particle-polymer composite that can be explored.

To overcome the material selection limitation and achieve simultaneous control of orientation and composition, this work investigated the use of acoustophoresis in stereolithography process, which is one of the most popular vat photopolymerization based additive manufacturing processes. Acoustophoresis has the advantages of full particle placement control, no imposed manufacturing constraints, and no material shape or specific physical property requirements [11-16]. Utilization of the acoustic field for particle patterning during additive manufacturing process has been reported in a few studies. 3D printing composite filaments consisting fillers through an acoustically-excited microfluidic print nozzle was demonstrated by Collino et al. while clogging issue remained to be solved [17]. Scholz et al. manufactured a thin layer of fiber reinforced polymer composites via the process of

ultrasonic assembly followed by polymerization [18]. Nonetheless, post-processing of laser cutting was required to obtain samples with desired geometries. By employing a near-UV laser for polymerization, Llewellyn-Jones et al. successfully printed composites that contained ultrasonically arranged glass fibers with desired geometries, but had difficulties in multiple layer fabrication [19]. Yunus et al. printed parts with acoustically assembled lines of electrically conductive particles for electronic applications, yet had restrictions on monotonous particle pattern [20]. In sum, current acoustophoresis techniques have limitations in forming various patterns of particles. The formed patterns of particles are limited to unidirectional parallel lines. Hence, pattern diversity needs to be expanded. Additionally, in acoustophoresis related literature, only particle with certain size range has been successfully manipulated to form patterns [19-23]. Broadening particle size range provides opportunities to fabricate composites with varied properties and functions.

In this paper, we developed an acoustic field-assisted projection stereolithography (A-PSL) process, characterized by a layer-by-layer in-situ particle pattern formation, capability of fabricating smart polymer composite products with heterogeneous properties. With the assistance of an external acoustic field, it is possible to control dispersion pattern of particles in liquid photopolymer, and hence to fabricate material intelligence by patterning particles and localizing particle concentrations in the polymer matrix. The machine design was studied to improve the distribution pattern controllability. A testbed which integrated acoustophoresis and stereolithography was built. Four test cases were fabricated and analyzed to verify the feasibility of the proposed process on fabricating particle-polymer composites with heterogeneous properties.

2. Method and Material

2.1 A-PSL Setup

Figure 1A illustrates the proposed A-PSL system. The main components include a resin vat, several piezoelectric elements, an imaging unit, and a platform which is driven by a Z stage. The resin vat holds the pre-mixed suspension of particle and photocurable polymer. Piezoelectric elements provide an acoustic field for patterning particles in the liquid resin. The imaging unit exposes patterned light according to the digital mask converted from the sliced cross-section of the 3D model. Cured layer is built on the platform after the mask image projection. Z stage drives the platform along the Z direction.

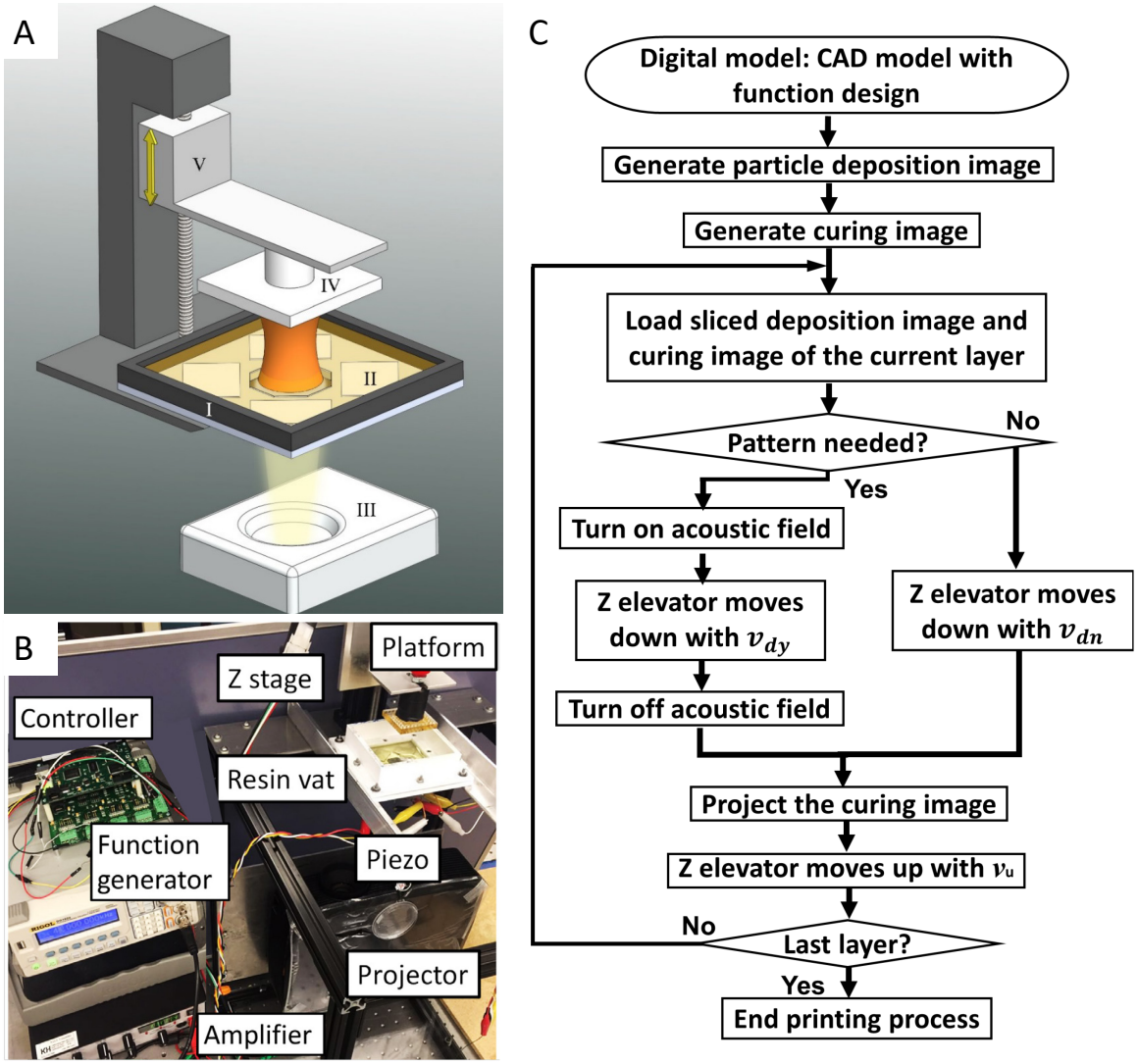

Figure 1. The A-PSL system: (A) Printer schematic detailing the main components: I. resin vat II. piezoelectric element III. image unit IV. platform V. linear actuator. (B) The prototype machine of A-PSL. (C) Flowchart of the manufacturing process.

A prototype machine was built to implement the proposed A-PSL process. As shown in Fig.1B, it consists of an off-the-shelf projector as imaging unit, a linear stage that elevates the build platform along the Z direction, a motion-controller that controls the linear stage, and a resin vat with embedded piezoelectric elements. The base of the resin vat has a window for light passing through. The printing envelop size is determined by the dimension of this window. The top of the base is covered by a transparent polyethylene terephthalate (PET) film. Four piezoelectric elements are placed horizontally underneath the film at each corner of the vat. A function generator provides the sinusoidal signal at 43 KHz with 5 volts peak to peak voltage. This signal is amplified by an amplifier and then applied to piezoelectric elements.

2.2 Manufacturing process

The proposed acoustic field assisted stereolithography process is illustrated in Fig. 1C. A digital model with both geometric information and particle pattern information is used to generate particle deposition images and curing images. Particle deposition images provide required information including filling patterns and areas for filling particles in the polymer matrix properly. The curing image is a digital mask converted from cross section geometry. For each layer, particle deposition image and curing image will be loaded into the main process control program. If the particle deposition image indicates that no particle distribution pattern is needed for the current layer, Z elevator moves down with a relatively fast velocity V_{dn}, to form a layer of uniformly suspended particle-polymer suspension for curing. If the deposition image indicates that the current layer needs to be filled with a particles distribution pattern, piezoelectric elements will be actuated to redistribute particles to the desired pattern. Next, the Z stage moves down with a velocity V_{dy} to create a layer of resin with patterned particles. V_{dy} is smaller than V_{dn} for preventing disturbing the particle distribution pattern. After turning off the acoustic field, the curing image will be projected to cure the mixture. Curing time for the

particle-polymer mixture was found to be dependent on particle loading fraction in our previous study [9]. Higher particle loading fraction requires a longer curing time to achieve the desired curing depth and layer thickness. Furthermore, the relationship between the loading fraction and curing time is not simply linear. In this study, curing depth experiments as described in our previous study [9] were performed to identify the appropriate curing time for each particle-polymer suspension recipe and layer thickness. Z stage drives the platform up with a speed V_u for the fresh resin to refill after one layer is solidified. A 3D heterogeneous particle-polymer composite product with desired geometries and particle distribution patterns is then built in a layer-by-layer fashion by repeating this procedure. During this process, the local composition and particle distribution pattern are precisely controlled through programming the externally applied acoustic field. Hence local particle distribution control and heterogeneous properties are possible to be achieved.

2.3 Material

SPOT-E elastic (Spot-A Materials, Sonnaya Ulitka S.L., Barcelona, Spain), a photocurable resin, was selected as the base resin in this study. Observing the particle distribution inside polymer calls for a translucent color base resin. Additionally, the flexibility of this base resin after solidification allows the cured part to be bended or deformed. In this study, four types of particles including tungsten (US Research Nanomaterials, Inc., TX, USA), aluminium (Alpha Chemicals, MO, USA), titanium (Sigma-Aldrich, MilliporeSigma, MO, USA) and copper (Sigma-Aldrich, MilliporeSigma, MO, USA) were tested. Those selected particles cover a wide range of particle sizes from 70 nm to 75 μm. In addition, they have multiple functionalities and hence can add different functions to the composite, which open possibility for future application of the printed composite. Properties of particles are summarized in Table 1. Suspensions of the base resin and filler particles with a weight loading fraction of 2.5% were homogenized by using a AR-100 conditioning mixer (Thinky U.S.A.,

Inc., Laguna Hills, CA, USA). After the planetary centrifugal mixing process at revolution speed of 1500 rpm for 10 minutes, the resulting mixture was used as feed stock for fabricating all parts.

Table 1. Particle properties.

Particle	Tungsten	Aluminum	Titanium	Copper
Size (μm)	0.07	30	45	75
Density (g/cm^3)	19.25	2.70	4.51	8.96

3. Multiphysis Simulation

3.1 Force analysis

The acoustic radiation force F_r on a spherical particle with radius much smaller than the wavelength λ in a nonviscous fluid can be expressed as Eq. 1 [24]:

$$F_r = -\frac{2\pi V_p E_{ac}}{\lambda} \emptyset \sin(\frac{4\pi x}{\lambda}) \quad (1)$$

where V_p is the volume of the particle, E_{ac} is the acoustic energy density as listed in Eq. 2:

$$E_{ac} = \frac{p_a^2 \beta_f}{4} \quad (2)$$

where p_a is the acoustic pressure, β_f is the compressibility of the fluid.

$\emptyset$ is the contrast factor as shown in Eq. 3:

$$\emptyset = \frac{5\rho_p - 2\rho_f}{2\rho_p + \rho_f} - \frac{\beta_p}{\beta_f} \quad (3)$$

where ρ_p is the density of the particle, ρ_f is the density of the liquid, β_p is the compressibility of the particle.

Radiation force drives particles towards a pressure node from a pressure anti-node. During travel in the fluid, particles in the liquid resin experience Stokes drag force F_d [15]:

$$F_d = 6\pi\mu r v_p \tag{4}$$

where μ is the dynamic viscosity of the liquid and v_p is the velocity of the particle. It can be seen from Eq. 4 that by selecting base resin with low viscosity, undesired drag force can be reduced, which will make it possible to pattern particles with a lower power.

3.2 Numerical model

The numerical model of the A-PSL setup was implemented and solved by using finite element software COMSOL Multiphysics 5.2a. Fig. 2A shows the geometry and material choices for the finite element model (FEM) to reflect the experimental setup of A-PSL. In the FEM model, a PET film (l: 77.4 mm, w: 77.4 mm, h: 0.13 mm) is inserted between a layer of resin (h: 2mm) and four piezoelectric plates (l: 20 mm, w: 15 mm, h: 1 mm). "Solid Mechanics – Linear Elastic Materials" physics was applied to the PET domain, "Solid Mechanics – Piezoelectric Materials" and "Electrostatics" physics were applied to the piezoelectric transducer (PZT) domain, and the "Pressure Acoustics" and "Particle Tracing for Fluid Flow" physics were assigned to the resin domain. Boundary condition setups are discussed in the following: the bottom surface of the PZT was set to "roller" condition, the interface between PZT and PET was coupled, the interface between PET and resin was set to "Acoustic-Structure Boundary", the rest boundaries of PET and PZT were set to "free" condition, and the rest boundaries of resin was set to "Sound Hard Boundary".

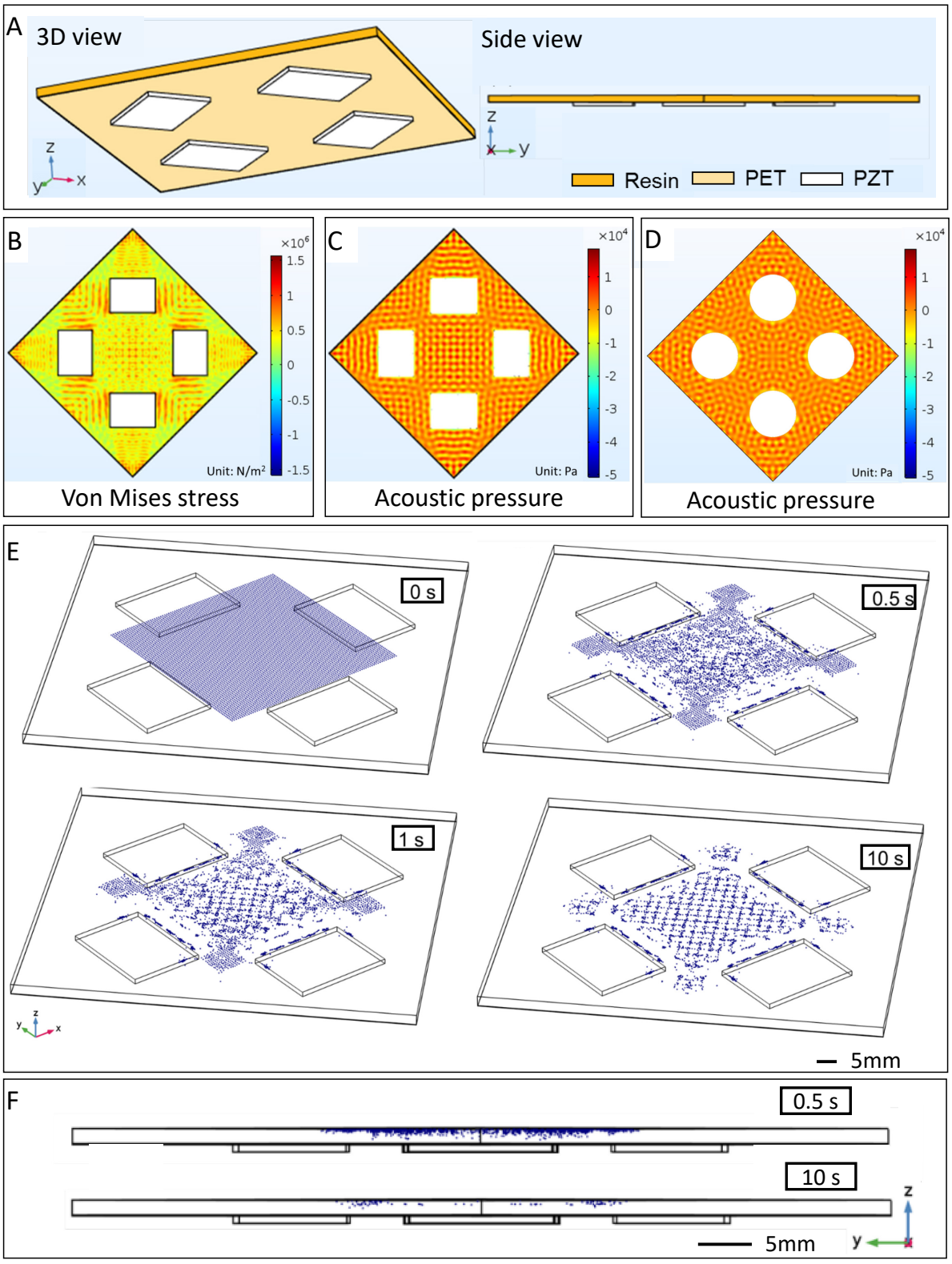

Figure 2. Multiphysis simulation: (A) The FEM model of the A-PSL setup detailing material choice in various views. (B) Frequency domain simulation results for the von Mises stress of the PET (C) Numeral simulation of acoustic pressure field patterns produced by piezoelectric plates. (D) Numeral simulation of acoustic pressure field patterns produced by piezoelectric disks. (E) Snapshot of particle distribution taken from the x-y-z isotropic view at 0 s, 0.5 s, 1 s, and 10 s. (F) Snapshot of particle distribution taken from the y-z plane at 0.5 s and 10 s.

To simulate the case when all four PZTs are “on”, a sinusoidal voltage with 100 V amplitude and 43 kHz frequency was applied to the bottom surface of the PZTs, while their top surface was set to “ground”. A frequency domain study computed the stress of the PET and the acoustic pressure distribution inside the resin domain, both of which are caused by the PZT actuation. Fig. 2B shows the von Mise stress of the PET and Fig. 2C shows the acoustic pressure of the resin produced by piezoelectric plates when viewed from the x-y plane along the positive direction of the z-axis. The stress pattern matches very well with the acoustic pressure pattern, indicating that the PZT actuation results in structural deformation of the PET film, which subsequently induces an acoustic field in the resin.

To investigate the effect of piezo element shape on acoustic pressure patterns, the numerical simulation of the A-PSL setup using four piezo disks (d: 20 mm, h: 1 mm) was also performed with COMSOL simulation. The piezoelectric plate and piezoelectric disk were defined with the same piezoelectric materials but they differed in shapes and dimensions. The analytical equations (Eq.1-4) apply to both piezo plate and piezo disk. Numeral simulation of acoustic pressure field patterns produced by piezo disk is shown in Fig. 2D. Based on the comparison between Fig. 2C and 2D, it is clear that difference in piezo element shapes will result in different acoustic pressure patterns and consequently produce different spatial distribution of suspended particles as shown in Figure S1.

After the acoustic pressure has been computed from the frequency-domain study, a time-domain study (starting at 0s and stops at 10s) was conducted to compute the trajectory of the particles dispersed inside the resin domain. The aluminum particles and the Spot-E resin were used as model materials for the simulation. The particle and resin properties are listed in Table 2. The forces applied to the particle include the acoustic radiation force (calculated from the acoustic pressure using Eq. 1-3), the drag force (calculated from Eq. 4), and the gravity

force. The particle suspension is modelled as monodispersed with no particle-to-particle interaction. Fig. 2E shows the snapshot of particle distribution at 0s, 0.5s, 1s, and 10s of the time-domain simulation. All snapshots are taken from the isotropic x-y-z view. The video showing the evolution of particle distribution with time is included in the Supplemental Information. It can be clearly seen that the particles form a grid-type pattern following the grid-type acoustic pressure pattern. Fig. 2F shows the snapshots of particle distribution taken from the y-z plane at 0.5s and 10s: the initially suspended particles dropped to the bottom of the resin due to gravity as demonstrated by the sparser suspended particles at 10s compared to 0.5s.

Table 2. Particle and resin properties used in the simulation.

Particle	Density	Size	Bulk modulus
	2700 kg/m^3	30 μm	68 GPa
Resin	Density	Dynamic viscosity	Speed of sound
	1120 kg/m^3	0.05 Pa-s	2230 m/s

In sum, the proposed method can locally pattern the particles in three-dimensional space. The piezo elements will generate standing acoustic wave (SAW) patterns on the x-y plane. The acoustic radiation force (given by Eq.1-2) will move the particles to the acoustic nodes at the lowest amplitude indicated by the yellow colored regions in acoustic pressure field patterns (Fig. 2C and 2D) or the acoustic antinodes at the highest amplitude represented by the red colored regions in Fig. 2C and 2D, depending on the density and compressibility of the particles. As shown in the simulation results of Fig. 2E, at equilibrium, the originally uniformly dispersed particles will be redistributed following the SAW patterns and thus achieving localized particle pattern on the x-y plane. The localized control of particle pattern along the z-axis is achieved by the layer-by-layer manufacturing process. Note that each layer is parallel to the x-y plane. Hence, by varying the SAW patterns on each layer, the proposed method can

also locally control the distribution of particles along the z axis and hence produce complicated 3D particle distribution patterns.

4. Results and Discussion

4.1 Particle patterning

As indicated by the analytical model and numerical model, the particle dispersion pattern is dependent on piezo element related parameters including shape, number, and layout, and process related parameters including frequency (i.e. wavelength) and magnitude of power, and/or using piezo element of different shapes (see Fig. 2D, showing that circular piezo elements generate different standing acoustic wave patterns that rectangular elements do) or different combination of shapes, and/or by arranging the locations of the piezo element differently, many more standing acoustic wave patterns (and thus particle distribution patterns) can be generated. Existing literature on acoustophoresis also showed that arbitrarily particle patterns are possible to be achieved by adjusting the acoustophoresis setup and process settings [25-29].

To test the capability of redistributing particles into different patterns using acoustic field in stereolithography systems, experiments have also been designed and performed. Five example patterns are given in Fig.3. In this set of experiments, two sets of piezo elements including four piezo plates and four piezo discs were arranged in diagonally symmetric way with the applied signal at 43 kHz frequency and 5V. Five configurations for each piezo elements set were tested and the resulting particle patterns are summarized in Fig. 3A.

A rectangular shape piezo plate patterns particles to form parallel lines while a round shape piezo disc forms concentric curves. The basic pairings of piezo elements are the opposite pair and the adjacent pair. With an opposite pair, parallel lines or concentric curves formed by each piezo element are overlapped in the center region. By adjusting the distance between two

opposite piezo elements, the overlapping can be eliminated or enhanced. By widening the distance, this configuration can be used to create patterns covering a larger area. By narrowing the distance, a denser pattern can be formed. With an adjacent pair, particles are patterned to crisscross of lines or curves. In addition, an opposite pair and an adjacent pair can be actuated simultaneously to obtain combined patterns.

Microscopic images in Fig. 3B present various micro-dispersion particle patterns embedded in the polymer matrix. Parallel lines and concentric curves were assembled by the piezo plate and disc, respectively. Crisscross patterns consisting of lines and curves were generated by the adjacent pair of piezo plates and discs, respectively.

Moreover, four types of particles, tungsten, aluminum, titanium, and copper, were tested and successfully assembled into desired patterns by actuating the corresponding configuration of piezo elements on the A-PSL setup. It demonstrates the capability of patterning various particles with a wide particle size ranging from 70 nm to 75 μm.

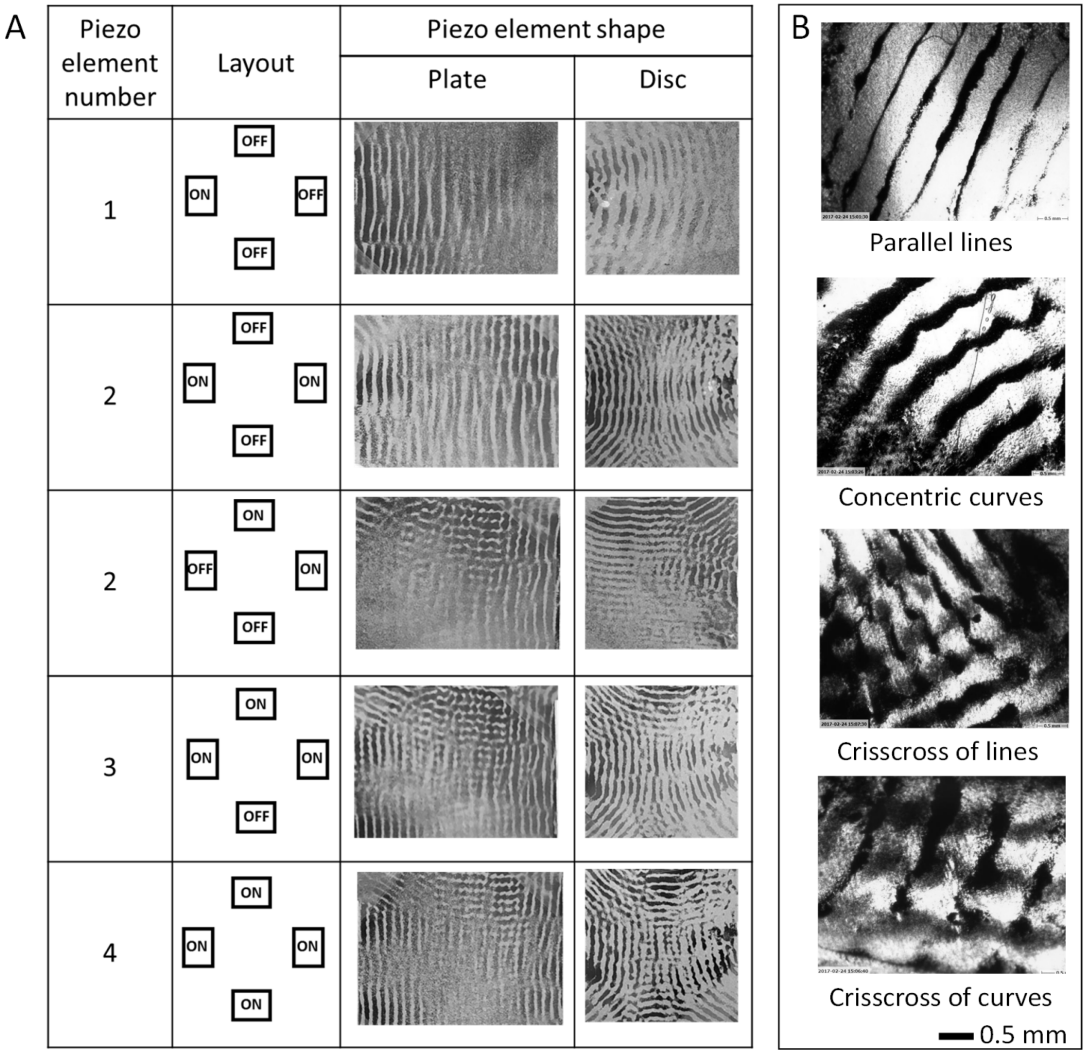

Figure 3. Various particle patterns: (A) Five configurations of piezo elements and the resulting particle patterns in the liquid resin, grey: aluminium particles (30 μm), black: SPOT-E elastic resin on black background. (B) Microscopic images of particle patterns embedded in the polymer matrix, black: tungsten particles (75 nm), white: cured SPOT-E elastic resin.

4.2 Micro-structure of particle assembly

To further observe the micro-structure of particle assembly embedded in the polymer matrix, microscopic images and scanning electron microscope (SEM) images of an acoustically assembled particle line have been taken. The inset in Fig. 4 shows a microscopic image of a line pattern. The line pattern sample was cut along the red dashed line using a blade. The cut plane, which is the cross sectional plane that is perpendicular to the alignment axis of the

particles, was coated with Platinum/Palladium (Pt/Pd) using E5100 sputter coaters (Polaron Equipment Ltd, Hertfordshire, England), and then observed under the S-3000N SEM (Hitachi High-Tech Instruments Co., Kumagaya, Japan). As can be seen in the SEM image in Fig. 4, the particles were assembled intensively into a line with a high particle density and an oval cross-section shape. The line cluster of acoustically assembled aluminum particles is measured to be approximately 150 μm in height and 400 μm in width. It is reported that the dimension of formed acoustic strap depends on particle loading fraction [17]. Hence the size of the formed line can be adjusted by changing particle loading fractions.

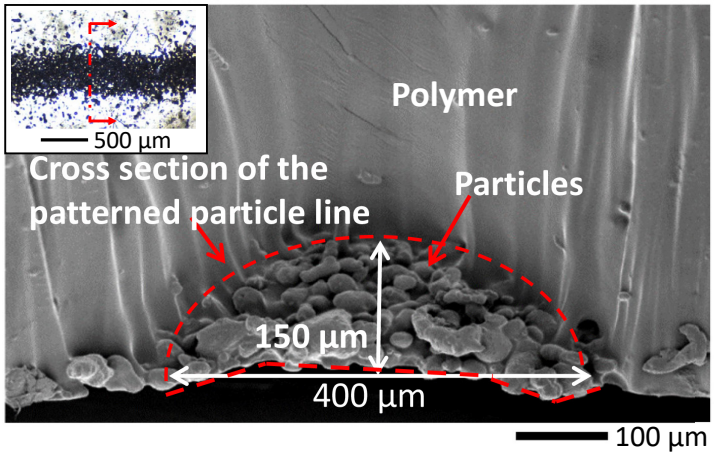

Figure 4. SEM image of the cross-section plane of a particle-polymer composite structure. Inset: An image of the acoustically assembled particle line in polymer matrix, black: aluminium particles (30 μm), white: cured SPOT-E elastic resin.

4.3 Printed results

To test the feasibility of integrating acoustic-field-assisted particle patterning with the layer-by-layer stereolithography based 3D printing process, four particle-polymer composite objects with simple geometries but different particle distribution designs were fabricated in the A-PSL setup with four rectangular shape piezo plates. The CAD models are presented in Fig. 5. The first object is a single layer part consisted of unidirectional parallel lines of particles. The second part contains a crisscross pattern. The third part is composed of orthogonally aligned particle lines within one layer. The fourth one is a multiple layered part with

unidirectional aligned particle lines on each layer. The orientation of lines on two neighboring layers are perpendicular. As shown in Fig. 5, the employed acoustic field layouts for pattern formation are illustrated in schematics. Printed results for each test case are summarized in Fig. 5.

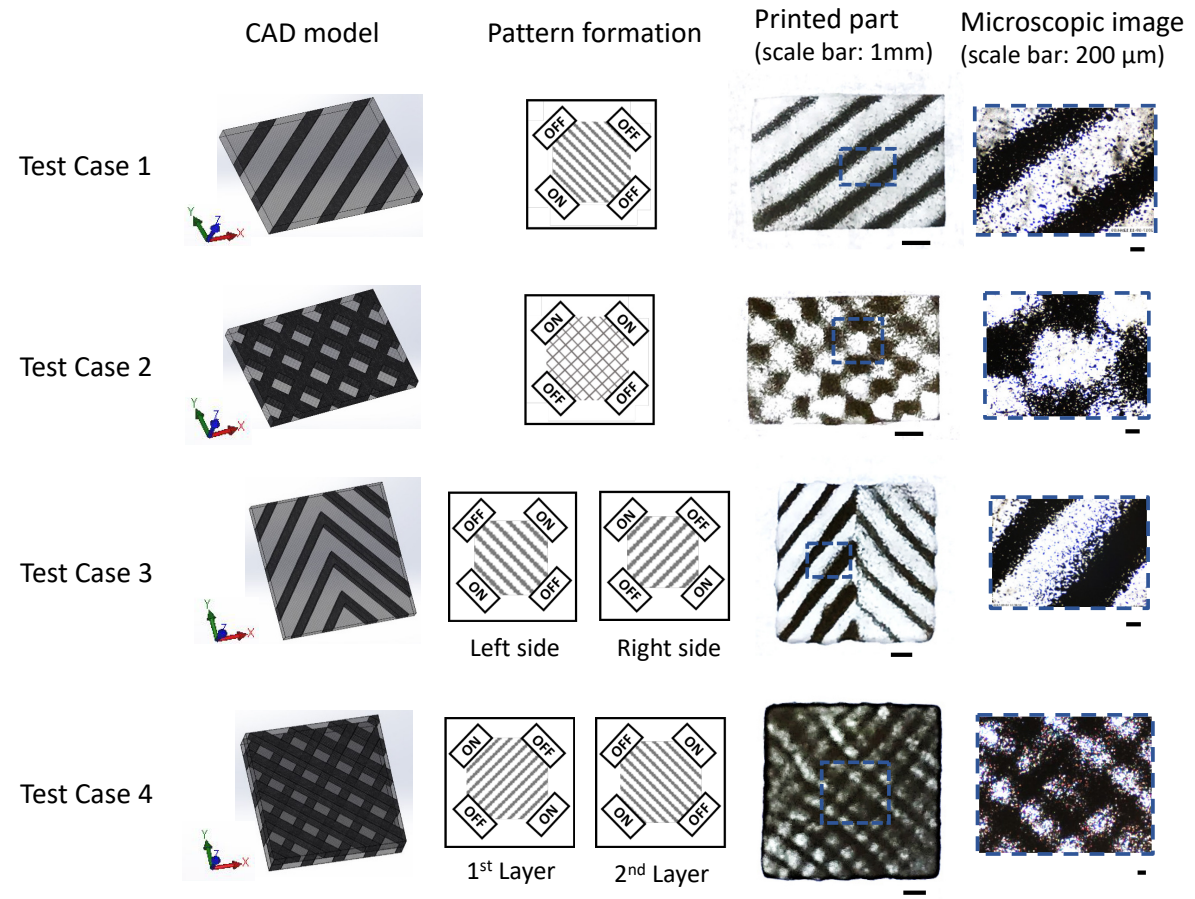

Figure 5. Test cases detailing with CAD models, patterns formation, photographs and microscopic images of printed parts. Black: aluminium particles (30 µm), clear: cured SPOT-E elastic resin.

Test case 1: a single layer part with uniform line pattern

A block shape part with unidirectional parallel lines covered the entire layer was fabricated. One piezo element was utilized to create the desired particle distribution pattern. From the photograph and the microscopic image of the fabricated part in Fig. 5, continuous particle distribution patterns can be observed. It shows the capability of the proposed acoustic

field-assisted process on fabricating particle-polymer composites with lined particle distribution patterns.

Test case 2: a single layer part with crisscross pattern

A cuboid part in Fig. 5 was designed to embed particles with a crisscross pattern. As aforementioned, crisscross pattern can be obtained by utilizing multiple piezo elements involving adjacent pair. In this test case, the crisscross pattern was formed by activating an adjacent pair. Crisscross pattern can be observed from the fabricated part in Fig. 5.

Test case 3: part with different patterns at different regions of one layer

A cuboid with square cross-section was tested as the third case. The particle dispersion pattern was designed to be different on the two halves of one part as shown in Fig.5. To realize the designed particle patterning, two pairs of opposite piezo elements were actuated one by one. The first pair of opposite piezo elements was turned on to form unidirectional lines. Then the left half of the layer was cured. Next, the second pair of opposite piezo elements were actuated to form lines in different orientation on the right side. Last, the remaining area was solidified by projecting the related mask image. From the printed result shown in Fig.5, it can be seen that particles are well distributed with an orthogonally lined pattern within the same printed layer.

Test case 4: part with orthogonally aligned reinforcement

To test the capability of fabricating multi-layered particle-polymer composites in a layer-by-layer way, a multiple layered cuboid part with square cross-section was printed. Cross particle distribution pattern was designed as shown in Fig.5. For each layer, one pair of opposite piezo elements was actuated to form uniform oriented lines. By actuating two different pairs of piezo elements, the orientation of lines on each layer is formed with an angle of 90 degrees. Crisscross pattern can be observed from microscopic images in Fig. 5. It is verified that

proposed manufacturing process can be used to print multiple layers with different particle patterns in each layer.

5. Conclusions

An acoustic field-assisted projection stereolithography process was successfully developed for fabrication of heterogeneous particle-polymer composite. Assisted by an external acoustic field, dispersion pattern of particles in the liquid photopolymer can be planned and controlled. Various particle distribution patterns were formed and embedded in the polymer matrix. Four test cases with different particle distribution patterns were fabricated to demonstrate the feasibility of the proposed acoustic field-assisted AM technology on the production of particle-polymer composites with locally controlled particle distributions.

Future work will include: (1) Further investigate the effect of process settings and acoustic field parameters on particle distribution parameters, to achieve more accurate particle distribution control and more complicated particle distribution patterns. (2) Investigate anisotropic property of the printed composites including mechanical property and thermal property.

Acknowledgements

This material is based upon work supported by the National Science Foundation under Grant No.1663399.

Author Disclosure Statement

No competing financial interests exist.

Reference

[1] Tian X, Liu T,engfei L, Yang C, et al. Interface and performance of 3D printed continuous carbon fiber reinforced PLA composites. Compos Part A: Appl Sci Manuf, 2016;88:198-205.

[2] Yang Y, Chen Z, Song X, et al. Biomimetic anisotropic reinforcement architectures by electrically assisted nanocomposite 3D printing. Advanced Materials, 2017;29:11:1605750.

[3] Castles F, Isakov D, Lui A, et al. Microwave dielectric characterisation of 3D-printed BaTiO3/ABS polymer composites. Sci Rep, 2016;6:22714.

[4] Kokkinis D, Schaffner M, Studart A.R. Multimaterial magnetically assisted 3D printing of composite materials. Nat Communications, 2015;6:8643.

[5] Compton B. G, Lewis J. A. 3D-Printing of lightweight cellular composites. Advanced Materials, 2014;26:34:5930-5935.

[6] Kokkinis D, Schaffner M, Studart A.R. Multimaterial Magnetically Assisted 3D Printing of Composite Materials. Nat. Commun., 2015; 6:8643.

[7] Joshua J. Martin, Brad E. Fiore & Randall M. Erb, Designing bioinspired composite reinforcement architectures via 3D magnetic printing. Nature Communications, 2015; 6:8641.

[8] Lu L, Guo P, Pan Y. Magnetic-field-assisted projection stereolithography for three-dimensional printing of smart structures. Journal of Manufacturing Science and Engineering, 2017;139:071008-1.

[9] Lu L, Joyee E. B, Pan Y. Correlation between micro-scale magnetic particle distribution and magnetic-field-responsive performance of 3D printed composites. Journal of Micro- and Nano-Manufacturing, 2018;6:1:10.1115.

[10] Pan Y, Patil A, Guo P, et al. A novel projection based electro-stereolithography (PES) process for production of 3D polymer-particle composite objects. Rapid Prototyping Journal, 2017;23:2:236-245.

[11] Naseer S. M, Manbachi A, Samandari M, et al. Surface acoustic waves induced micropatterning of cells in gelatin methacryloyl (GelMA) hydrogels. Biofabrication, 2017; 9:015020.

[12] Kapishnikov S, Kantsler V, Steinberg V. Continuous particle size separation and size sorting using ultrasound in a microchannel. J. Stat. Mech., 2006;1:1-15.

[13] Petersson F, Lena Aberg L, Swärd-Nilsson A-M, et al. Free flow acoustophoresis: microfluidic-based mode of particle and cell separation. Anal. Chem., 2007; 79:14:5117-5123.

[14] Kuznetsova L. A, Martin S. P, Coakley W. T. Sub-micron particle behaviour and capture at an immuno-sensor surface in an ultrasonic standing wave. Biosensors and Bioelectronics, 2005;21:6:940-948.

[15] Koklu M, Sabuncu A. C, Beskok A. Acoustophoresis in shallow microchannels. J. Colloid Interface Sci., 2010;351:2:407-414.

[16] Coakley W. T, Bardsley D. W, Grundy M. A, et al. Cell manipulation in ultrasonic standing wave fields. J. Chem. Tech. Biotechonol., 1989;44:43-62.

[17] Collino R. R, Ray T. R, Fleming R. C, et al. Deposition of ordered two-phase materials using microfluidic print nozzles with acoustic focusing. Extreme Mechanics Letters, 2016;8: 96-106.

[18] Scholz M.-S, Drinkwater B. D, Trask R. S. Ultrasonic assembly of anisotropic short fibre reinforced composites. Ultrasonics, 2014;54:4:1015-1019.

[19] Llewellyn-Jones T. M, Drinkwater B. D, Trask R. S. 3D printed components with ultrasonically arranged microscale structure. J. Smart Material Structures, 2016;25:2:02LT01.

[20] Yunus D. E, Sohrabi S, He R, et al. Acoustic patterning for 3D embedded electrically conductive wire in stereolithography. Journal of Micromechanics & Microengineering, 2017; 27:4.

[21] Van Neer P.L.M.J, Rasidovic A, Volker A.W.F. A study of nanoparticle manipulation using ultrasonic standing waves Ultrasonics Symposium (IUS), 2013 IEEE International. DOI: 10.1109/ULTSYM.2013.0488.

[22] Shi J, Ahmed D, Mao X, et al. Acoustic tweezers: patterning cells and microparticles using standing surface acoustic waves (SSAW). Lab Chip, 2009; 9:2890-2895.

[23] Wood C. D, Evans S. D, Cunningham J. E, et al. Alignment of particles in microfluidic systems using standing surface acoustic waves. Appl. Phys. Lett., 2008; 92: 044104.

[24] Bruus H. Acoustofluidics 7: the acoustic radiation force on small particles. Lab on a Chip, 2012;6.

[25] Ding X, Li P, Lin S.-C. S, et al. Surface acoustic wave microfluidics. Lab Chip, 2013;13:18:3626, 2013.

[26] Ding X, Lin S.-C. S, Kiraly B, et al. On-chip manipulation of single microparticles, cells, and organisms using surface acoustic waves. Proc. Natl. Acad. Sci., 2012;109:28:11105–11109.

[27] Courtney C. R. P, Demore C. E. M, Wu H, et al. Independent trapping and manipulation of microparticles using dexterous acoustic tweezers. Appl. Phys. Lett., 2014;104:15:1–5.

[28] Melde K, Mark A. G, Qiu T, et al. Holograms for acoustics. Nature, 2016; 537:7621:518–522.

[29] Melde K, Choi E, Wu Z, et al. Acoustic Fabrication via the Assembly and Fusion of Particles. Adv. Mater., 2017;1704507.